Asymmetry of the Electrostatic Induction Coefficient Matrix Calculated using MoM

Evgeniya B. Chernikova
Department of Microwave and Quantum Radio Engineering
Tomsk State University of Control
Systems and Radioelectronics
Tomsk, Russian Federation
0000-0003-1964-7616

Van Dong Nguyen
Television and Control Department
Tomsk State University of Control
Systems and Radioelectronics
Tomsk, Russian Federation
thanhxuancuatoi1994@gmail.com

***Abstract*—This paper presents a study of the asymmetry of the off-diagonal elements of the matrix of electrostatic induction coefficients C (Maxwell capacitance matrix), computed using the method of moments in transmission line modeling. Using a strip structure enclosed in a metallic enclosure as an example, the influence of discretization parameters, as well as geometric and electrical parameters, on the accuracy of the computation is analyzed. It is shown that the observed asymmetry is not related to the physical asymmetry of the structure but arises from the specifics of the numerical implementation of the method. The analysis demonstrates that the asymmetry is significantly affected by the nature and uniformity of the geometry segmentation, the ratio of segment sizes in different regions of the structure, the conditioning of the system matrix, and the degree of electric field inhomogeneity determined by geometric and electrical parameters. It is also shown that a decrease in the dielectric permittivity of the medium leads to a reduction in asymmetry, and in the case of modeling a structure without a dielectric using autosegmentation, the elements of the matrix C coincide to the last significant digit.**

Keywords—radioelectronics, numerical modeling, transmission lines, strip structure, matrix of electrostatic induction coefficients, method of moments

I. Introduction

Strip transmission lines are an essential component of modern radio electronics and are widely used in signal transmission and processing devices. In addition, they serve as the basis for various microwave components, including filters, directional couplers, antennas, and protective devices with modal decomposition. The design of such devices is largely determined by the properties of the employed strip structures, which are often analyzed using a quasi-static approach assuming quasi-TEM wave propagation [1]. Within this approximation, the primary per-unit-length parameters of a transmission line can be determined by solving an electrostatic problem reduced to the Poisson/Laplace equations [2]. Various numerical methods are used to solve these equations [3], among which the method of moments (MoM) is one of the most widely applied [4]. In the TUSUR.EMC software, the electrostatic induction coefficient matrix **C** (Maxwell capacitance matrix) is computed using a numerical solver based on the MoM solution of the electrostatic problem [5]. This approach involves determining the surface charge density distribution $\sigma(r)$ on the boundaries of conductors and dielectrics, which is then used to calculate capacitances [6]. The diagonal elements of the Maxwell capacitance matrix are the loaded capacitances of each conductor. It is not just the capacitance to the return path, the ground reference, it is the capacitance to the return path and to all the other conductors that are also tied to ground [7]. The off-diagonal elements of the matrix of electrostatic induction coefficients are negative, as they reflect the magnitude of the negative induced charge on a grounded conductor when a positive potential is applied to an adjacent conductor.

$$\mathbf{C}=\begin{bmatrix} c_{11} & -c_{12} & \cdots & -c_{1j} \\ -c_{21} & c_{22} & \cdots & -c_{2j} \\ \vdots & \vdots & \ddots & \vdots \\ -c_{i1} & -c_{i2} & \cdots & c_{ij} \end{bmatrix}.$$

In general, the elements of the matrix **C** must be equal relative to the main diagonal; that is, the matrix **C** possesses symmetry of mutual elements ($c_{ij}=c_{ji}$) [8]. However, when studying certain types of structures, an asymmetry of the off-diagonal elements of the matrix **C** can be observed. This effect is particularly evident, for example, in the case of a two-conductor transmission line placed in a metallic enclosure [9]. The asymmetry of the matrix **C** directly affects the analysis of real microwave devices (such as filters), since it represents the matrix of primary per-unit-length parameters from which all secondary line parameters are derived. In quasi-static analysis, this is critically important, as the accuracy of the primary parameters directly determines the precision of the calculated characteristic impedances, coupling coefficients, and signal delays, without which it is impossible to obtain a correct response of the designed device.

The occurrence of asymmetry may be attributed to a number of factors related both to the specifics of the numerical implementation of the MoM and to the parameters of the structure under consideration. These factors include the method of boundary discretization (segmentation), the choice of basis and weighting functions, the specifics of taking into account boundary conditions, as well as the geometric and electrical parameters of the model. Therefore, a detailed analysis of the causes of asymmetry in the matrix **C**, as well as an assessment of the influence of various factors on its manifestation, is required. The purpose of this work is to study the asymmetry of the off-diagonal elements of the electrostatic induction coefficient matrix computed using the MoM by varying discretization parameters and the geometry of the structure, and to analyze the influence of these factors on the degree of asymmetry.

This work was financially supported by the Ministry of Science and Higher Education of the Russian Federation under project FEWM-2024-0005.

II. Statement of the Problem

A. Structure under Study

The structure under consideration is a coupled microstrip transmission line placed inside a rectangular shielding enclosure. In this case, the shield is modeled as a signal conductor (Fig. 1), thus, the resulting matrix **C** has a dimension of 3×3. This approach allows variations in the enclosure potential to be taken into account and provides a more complete physical description of the system, although it introduces an additional mode whose field is predominantly concentrated in air. It is important to note that in this problem the shield acts not only as a passive conductor but also as an element that may be subjected to external excitation, since the study aims to investigate the influence of intentional interference propagating through grounding circuits. Therefore, representing the enclosure as a separate conductor is fundamentally necessary, and the electrical parameter matrix must have a 3×3 dimension. Numerical modeling of such a system system (line parameters: s=100 µm, w=300 µm, h=335 µm, t=35 µm, b=4200 µm, k=8300 µm, ε_r=4.5) using the MoM reveals a violation of the symmetry of the matrix **C**, which contradicts the expected physical properties of the model. In an alternative simulation, where the shield is treated as an ideal ground, its potential is fixed at zero, the matrix dimension is reduced to 2×2, and the numerical asymmetry does not appear, since interaction with the enclosure is effectively replaced by interaction with an infinite ground plane. However, this approach is less accurate, as it eliminates the possibility of accounting for excitation of the enclosure and obscures numerical features of its interaction with the signal conductors.

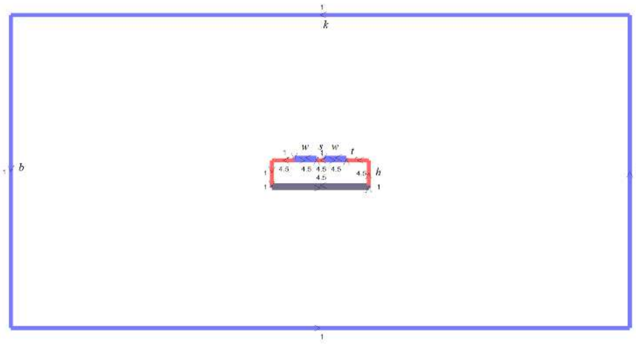

Fig. 1. Cross-section of the studied structure in the TUSUR.EMC software.

B. Computation of the *C* Matrix

The **C** matrix with autosegmentation at a step of 7 µm (5 segments on the edge of the signal conductor) is given as follows:

$$\mathbf{C}=\begin{bmatrix} 92.22 & -27.79 & -4.748 \\ -27.79 & 92.22 & -4.748 \\ -4.458 & -4.458 & 31.08 \end{bmatrix}\text{pF/m.} \qquad (1)$$

Thus, c_{13} represents the charge integral over the surface of conductor 1 (1 V is applied to the enclosure, which generates the field, and the charge is computed on conductor 1); c_{31} is the charge integral over the surface of the enclosure (1 V is applied to conductor 1, which generates the field, and the charge is summed over the enclosure surface); c_{23} is the charge integral over the surface of conductor 2 (1 V is applied to the enclosure, which generates the field, and the charge is computed on conductor 2); and c_{32} is the charge integral over the surface of the enclosure (1 V is applied to conductor 2, which generates the field, and the charge is summed over the enclosure surface). From matrix (1), it can be seen that $c_{13}=c_{23}$, and $c_{31}=c_{32}$, which is consistent, as the distance from conductor 1 to the enclosure is equal to that from conductor 2. Therefore, the electric field (and capacitive coupling) between conductor 1 and the enclosure is physically identical to that between conductor 2 and the enclosure. At the same time, the elements $c_{13}\neq c_{31}$, $c_{23}\neq c_{32}$. The deviation is calculated as:

$$\delta=\left|\frac{x_1-x_2}{x_1+x_2}\right|\times 100\%\,. \qquad (2)$$

where x_1 is the value of the first quantity and x_2 is the value of the second quantity.

As a result, the deviation δ between the elements c_{13} and c_{31} is 3.15 %.

III. Results Analysis of the Asymmetry Causes

A. Influence of Discretization

For an initial assessment of the influence of discretization on the asymmetry of the **C** matrix, simulations were performed using the coarsest possible geometric segmentation of a single segment:

$$\mathbf{C}=\begin{bmatrix} 71.04 & -27.79 & -4.125 \\ -27.79 & 71.04 & -4.125 \\ -5.698 & -5.698 & 34.11 \end{bmatrix}\text{pF/m.} \qquad (3)$$

From (3), it can be seen that the nature of the asymmetry persists, indicating that this effect is not directly related solely to the total number of segments.

For a more detailed analysis of the influence of discretization, a study was conducted that considered not only the total number of segments but also their distribution across the elements of the structure. It was assumed that non-uniform segmentation of different parts of the geometry could affect the accuracy of the electric field approximation in specific regions. To assess the impact of segmentation, additional calculations were performed using manual segmenting. The entire cross-section was divided into several sections, each segmented separately: *tor* is segments at the conductor edges, *mid* is segments across the width of the conductors, *verh* is segments on the top part of the enclosure, *niz* is segments on the bottom part of the enclosure, *bok* is segments on the side walls of the enclosure, and *dl* is segments on the dielectric.

The **C** matrix was computed for various manual segmentation configurations with a fixed number of segments dl=10 and tor=7. With uniform segmentation of the enclosure and conductor width (step of 20 µm), the deviation was δ=11%, whereas increasing the segmentation density of the enclosure to a 5 µm step reduced it to δ=10.1%. In the case of coarse segmentation of the enclosure (step of 200 µm) combined with finer segmentation across the conductor width (step of 20 µm), the deviation increased to δ=12.91%; conversely, with fine segmentation of the enclosure and coarser segmentation across the conductor width (step of 60 µm), the deviation was δ=11.8%. The results indicate that reducing the number of segments across the conductor width has a greater impact on the matrix elements associated with the signal conductors ($c_{11}=c_{22}$, $c_{12}=c_{21}$), while it has a minor effect on the deviation between c_{13} and c_{31}. Therefore, it is advisable to keep the segmentation across the conductor width fixed in further analysis. Increasing the overall segmentation density across the entire structure, including the enclosure, leads to a reduction in the deviation between c_{13} and c_{31} (as well as between c_{23} and c_{32}).

B. Influence of Geometry Segmentation

The results show that the magnitude of the asymmetry is influenced not only by the total number of segments but also by their distribution across the elements of the structure. Therefore, it is reasonable to examine the impact of segmenting individual parts of the structure separately.

To analyze the effect of enclosure segmentation, the **C** matrix was calculated for various manual segmentation configurations. The number of segments on the dielectric (*dl*=10), at the conductor edges (*tor*=7), and across the conductor width (*mid*=15) was kept fixed. The segmentation of the enclosure was varied sequentially for its individual parts. In particular, with a fixed number of segments on the top and bottom parts of the enclosure (*verh*=*niz*=415, step 20 μm), the segmentation of the side walls was varied with steps of 1, 5, 10, 20, 50, and 100 μm. Increasing the number of segments from 83 to 8300 led to a slight reduction in the deviation from 11.18 % to 10.6 %. Similarly, the segmentation of the top and bottom parts was varied while keeping the number of segments on the side walls fixed (*bok*=210, step 20 μm), resulting in only a minor change in the deviation from 12 % to 9.68 %.

To separately evaluate the influence of the top and bottom parts of the enclosure, calculations were performed by varying their segmentation sequentially (steps of 5, 20, and 100 μm) while keeping the segmentation of the remaining elements unchanged (*dl*=10, *tor*=7, *mid*=15, *bok*=210). The results indicate that the top and bottom parts of the enclosure contribute comparably to the overall deviation (≈11 %).

An analysis of the segmentation of the conductor edges was carried out by varying the segmentation step from 1 μm to 35 μm, while the segmentation of the rest of the geometry was kept fixed at a 20 μm step. The results are shown in Fig. 2.

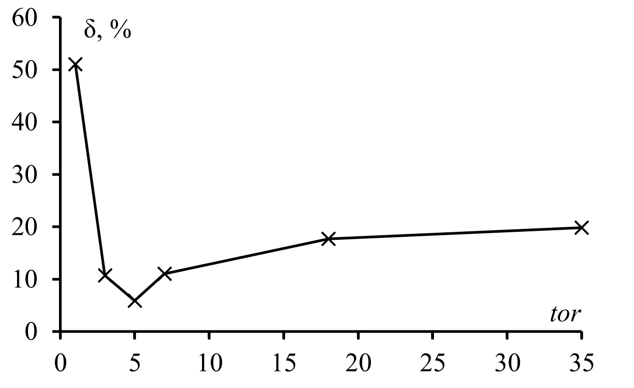

Fig. 2. Dependence of δ on the number of segments at the conductor edge.

A non-monotonic dependence of the deviation on the segment size was observed. This is explained by the disruption of grid uniformity and the resulting disproportion between the small segments at the conductor edges and the larger elements in other parts of the structure (in particular, on the enclosure with a 20 μm step). The large segments on the enclosure are unable to accurately capture the behavior of the electric field generated by the small segments at the conductor edges, leading to an increase in numerical errors in the **C** matrix. Furthermore, when the segments become very small (35 segments of 1 μm each), their centers become closely spaced. The rows of the matrix corresponding to adjacent micro-segments become nearly linearly dependent (the equations are almost identical), which increases the condition number of the matrix. When solving the system of linear equations, rounding errors accumulate. Combined with the size disproportion, this significantly increases the error. Thus, the minimum error is achieved with 5 segments, corresponding to an optimal configuration that balances the refinement of the charge distribution at the conductor edges with the numerical stability of the numerical solution.

To analyze the influence of dielectric segmentation, calculations were performed by varying the number of dielectric segments *dl* in steps of 2, while keeping the segmentation of the other elements fixed at a 20 μm step and *tor*=7 (Fig. 3). It was shown that increasing the number of segments reduces the deviation from 15.9 % to 10.25 % as *dl* increases from 1 to 14.

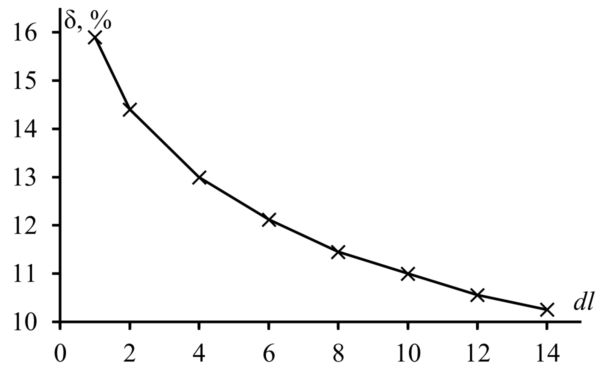

Fig. 3. Dependence of δ on the number of segments in the dielectric.

C. Influence of Geometric and Electrical Parameters

To analyze the effect of changing the coupling between the transmission line and the enclosure, the **C** matrices were computed with fixed segmentation parameters (*dl*=10, *mid*=15, *verh*=*niz*=415, *bok*=210) while varying the number of segments at the conductor edge (*tor*=5 and 7) and reducing the distance between the transmission line and the enclosure by half. The results are presented in Table I.

TABLE I. MATRICES **C** FOR VARYING THE DISTANCE BETWEEN THE ENCLOSURE AND THE TRANSMISSION LINE

tor	*b*, μm	C, pF/m	δ, %
5	4200	$\begin{bmatrix} 89.62 & -26.76 & -4.991 \\ -26.76 & 89.62 & -4.991 \\ -4.439 & -4.439 & 39.03 \end{bmatrix}$	5.85
	2100	$\begin{bmatrix} 90.53 & -26.09 & -7.681 \\ -26.09 & 90.53 & -7.681 \\ -7.233 & -7.233 & 56.35 \end{bmatrix}$	3
	1050	$\begin{bmatrix} 94.23 & -24.34 & -14.92 \\ -24.34 & 94.23 & -14.92 \\ -14.73 & -14.73 & 103.58 \end{bmatrix}$	0.64

tor	*b*, µm	C, pF/m	δ, %
	525	$\begin{bmatrix} 122.62 & -20.52 & -50.6 \\ -20.52 & 122.62 & -50.6 \\ -52.67 & -52.67 & 440.89 \end{bmatrix}$	2
7	4200	$\begin{bmatrix} 89.43 & -26.53 & -5.551 \\ -26.53 & 89.43 & -5.551 \\ -4.455 & -4.455 & 39.31 \end{bmatrix}$	11
	2100	$\begin{bmatrix} 90.34 & -25.86 & -8.228 \\ -25.86 & 90.34 & -8.228 \\ -7.243 & -7.243 & 56.55 \end{bmatrix}$	6.37
	1050	$\begin{bmatrix} 94.04 & -24.11 & -15.46 \\ -24.11 & 94.04 & -15.46 \\ -14.73 & -14.73 & 103.62 \end{bmatrix}$	2.42
	525	$\begin{bmatrix} 122.45 & -20.27 & -51.16 \\ -20.27 & 122.45 & -51.16 \\ -52.52 & -52.52 & 439.61 \end{bmatrix}$	1.31

The analysis showed that reducing the height of the enclosure (i.e., decreasing the distance between the enclosure and the transmission line) leads to the following effects:

- an increase in the self-capacitances of the conductors (c_{11} and c_{22}), since bringing the grounded enclosure closer to the conductors increases the flow of electrical displacement to the ground;
- a decrease in the mutual capacitances (c_{12} and c_{21}) due to the redistribution of the field lines, part of which now terminate on the enclosure;
- a significant increase in the capacitances to the enclosure c_{13} and c_{31} (c_{23} and c_{32}) as a result of strengthened electrostatic coupling.

Analysis of the deviation values from Table I showed that at a large distance between the enclosure and the transmission line (b=4200 µm), the deviation is maximal. At this distance, it is 5.85 % for *tor*=5 and 11 % for *tor*=7, indicating that finer segmentation increases the error. Bringing the enclosure closer reduces the deviation to 0.64 % and 1.31 %, respectively.

At the minimum separation between the enclosure and the transmission line (b=525 µm and h=335 µm), the deviation increases for *tor*=5 but decreases for *tor*=7. When the enclosure is very close, the electric field in the gap between the conductor edge and the enclosure wall becomes highly non-uniform, with a very steep potential gradient. In this regime (strong-coupling mode), 5 segments are no longer sufficient to accurately capture the sharp bending of the field lines. The need for a more detailed representation of the field outweighs the issues related to matrix conditioning, making a finer segmentation preferable in this case.

The analysis of c_{13} and c_{31} (c_{23} and c_{32}) showed that when the enclosure is brought closer, the capacitance increases by a factor of 11 (from 4.43 to 52.67 pF/m for *tor*=5 and from 4.45 to 52.52 pF/m for *tor*=7), while the absolute error in pF between c_{13} and c_{31} remains approximately constant (~1.1 pF for *tor*=7). This error becomes negligible compared to the large capacitance.

Thus, in the weak coupling regime, matrix conditioning dominates, and it is better to use a coarser mesh (*tor*=5) proportional to the other elements to avoid poor conditioning. In the strong-coupling regime, the accuracy of the field approximation becomes the dominant criterion, requiring a finer mesh (*tor*=7) to correctly capture the sharp variation of the field in narrow gaps.

As an additional factor potentially affecting the manifestation of asymmetry in the **C** matrix, the influence of the substrate relative permittivity ε_r was considered. Changing ε_r leads to a redistribution of the electric field within the structure, which can potentially impact the numerical solution accuracy and the magnitude of deviations between matrix elements. Calculations of the **C** matrix were performed using autosegmentation with steps of 5, 7, 11.6, 17.5, and 35 µm, corresponding to 7, 5, 3, 2, and 1 segment per conductor edge, respectively, for various values of ε_r. The results are presented in Table II and Fig. 4 (the plot for the 35 µm step is not shown due to incorrect matrix computation).

As a result, it was found that when the medium approaches air (ε_r=1.1), the deviation decreases to $\delta \approx 0.08$, meaning that the asymmetry virtually disappears. This is due to a more uniform distribution of the electric field and reduced sensitivity of the solution to discretization. As ε_r increases, a nonlinear growth in the maximum error is observed for all studied segmentation steps. This effect is explained by the redistribution of the electric field: the high permittivity of the substrate increases the field concentration at the interfaces between materials, requiring a finer computational mesh to adequately approximate the charge distribution.

TABLE II. MATRICES C WHEN TRANSMISSION LINE ER CHANGES

ε_r	5 µm	7 µm	11.6 µm	17.5 µm	35 µm
1.1	0.05	0.03	0.009	0.2	0.69
1.5	0.28	0.27	0.23	0.8	0.55
2.3	0.87	0.9	0.88	2.21	0.004
4.5	2.93	3.15	3.35	6.93	2.85
10.2	9.54	10.8	12.7	21.81	25.24
16	17.5	20.8	27.3	40.14	-
20	23.7	29.3	42.4	54.93	-

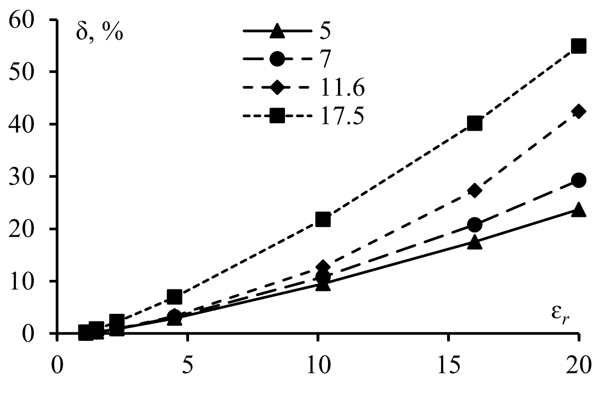

Fig. 4. Dependence of δ on the ε_r.

The study of the error dependence on the autosegmentation step revealed a direct correlation between the number of segments at the conductor edge and the stability of the numerical solution. The best accuracy across the entire range was achieved with a step of 5 µm (7 segments per edge). At the same time, using only one segment per edge (step of 35 µm) leads to a critical loss of accuracy. The computation of the matrix becomes mathematically incorrect (positive off-diagonal elements), confirming that excessive mesh coarsening is unacceptable when modeling structures with a high ε_r dielectric.

Additionally, simulations were performed for the structure without a dielectric (Fig. 5) using autosegmentation with a step of 5 µm. The resulting **C** matrix is as follows:

$$\mathbf{C}=\begin{bmatrix} 34.041 & -13.987 & -4.9959 \\ -13.987 & 34.041 & -4.9959 \\ -4.9959 & -4.9959 & 29.752 \end{bmatrix} \text{pF/m.} \qquad (4)$$

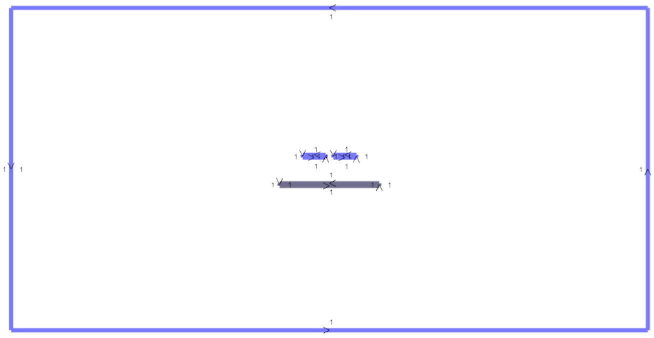

Fig. 5. Cross-section of the studied structure without a dielectric.

As a result, it was found that the elements of the **C** matrix presented in (4) match exactly, down to the last digit. This demonstrates that asymmetry appears only when a dielectric substrate is introduced. Therefore, it can be assumed that the primary cause of the numerical asymmetry is the use of a hybrid system of integral equations in the MoM implementation. While the interaction between conductors is described via a symmetric potential kernel, the boundary conditions on the dielectrics are formulated through the normal derivative of the Green's function. The difference in the mathematical nature of these kernels leads to a violation of reciprocity in the system of linear equations, manifesting as asymmetry in the resulting capacitance matrix, which becomes more pronounced as the dielectric permittivity increases.

IV. Conclusion

As a result, it was found that the asymmetry of the matrix **C**, observed in certain cases, is not related to the physical asymmetry of the structure but arises as a numerical effect when using the MoM. This effect is primarily caused by the non-uniformity of the mesh, which leads to a significant discrepancy in segment sizes on interacting conductors (micro-segments at the edges of signal lines versus large elements on the enclosure). Such a mismatch deteriorates the conditioning of the system matrix *S* and accumulates rounding errors during the solution of the linear system of equations, while also reducing the accuracy of the computed potential coefficients in cases where large segments fail to adequately approximate the non-uniform electric field generated by smaller segments. It was also established that a primary source of the asymmetry may be attributed to the hybrid formulation of the MoM, which uses the normal derivative of the Green's function kernel to describe dielectric boundaries.

To minimize asymmetry and improve accuracy, it is recommended to perform forced symmetrization of the matrix **C**. Future work will investigate the effect of increased computational precision on reducing accumulated rounding errors, as well as the influence of manual segmentation on the calculation of the matrix **C** for the structure without a dielectric.

References

[1] C. R. Paul, Analysis of multiconductor transmission lines, 2nd ed. Hoboken, New Jersey: John Wiley & Sons, 2008, 821 p.

[2] R. Garg and R. Mittra, Analytical and Computational Methods in Electromagnetics. Norwood, MA, USA: Artech House, 2008.

[3] M. N. O. Sadiku, Numerical techniques in electromagnetics, 2nd ed. Boca Raton, CRC Press, 2000, 760 p.

[4] R. F. Harrington, "Matrix methods for field problems," in *Proceedings of the IEEE*, vol. 55, no. 2, pp. 136-149, Feb. 1967, doi: 10.1109/PROC.1967.5433.

[5] A. E. Maksimov and S. P. Kuksenko, "Accurate Capacitance Matrices for Multiconductor Transmission Lines," in *IEEE Transactions on Electromagnetic Compatibility*, vol. 64, no. 5, pp. 1514-1521, Oct. 2022, doi: 10.1109/TEMC.2022.3175717.

[6] M. R. Scheinfein, O. A. Palusinski, "Methods of calculation of electrical parameters for electronic packaging applications," *Transactions of the society for computer simulation*, vol. 4, no. 3, pp. 187–254, Sept. 1987.

[7] E. Bogatin, Signal and power integrity – simplified, 2nd ed., Boston, MA: Pearson Education Inc., 2009, 757 p.

[8] M. B. Bazdar, A. R. Djordjevic, R. F. Harrington, and T. K. Sarkar, "Evaluation of quasi-static matrix parameters for multiconductor transmission lines using Gelarkin's method," *IEEE Trans. Microw. Theory Techn.*, vol. 42, no. 7, pp. 1223–1228, Jul. 1994, doi: 10.1109/22.299760.

[9] T. R. Gazizov, V. D. Nguyen and A. F. Alhaj Hasan, "Per-Unit-Length Matrixes of Shielded Coupled Microstrip Lines With Different Grounds," *2024 IEEE International Multi-Conference on Engineering, Computer and Information Sciences (SIBIRCON)*, Novosibirsk, Russian Federation, 2024, pp. 500-503, doi: 10.1109/SIBIRCON63777.2024.10758491.